1098 m, 1080 w, 1059 m, 993 w, 984 w, 889 w, 788 w, 747 s, 701 m, 690 m, 608 m, 508 w, 481 m cm^{-1}; UV (Ar, 15 K) λ_{max} 500, 312, 302, 298 sh, 280, 245, 235, 228, 222 nm. The deep-red diazo compound was sublimed at -23 °C (10^{-6} Torr) and codeposited with argon to form a matrix.

***p*-Methoxyacetophenone tosylhydrazone** was prepared from *p*-methoxyacetophenone (Aldrich) in 89% yield: mp 166-168 °C dec: ^1H NMR ($CDCl_3/Me_2SO$-d_6) δ 2.17 (s, 3 H), 2.38 (s, 3 H), 3.75 (s, 3 H), 6.82 (AB, 2 H, J = 9 Hz), 7.30 (AB, 2 H, J = 8 Hz), 7.54 (AB, 2 H, J = 9 Hz), 7.82 (AB, 2 H, J = 8 Hz), 10.23 (s, 1 H); mass spectrum (16 eV), m/z (relative intensity) 318 (M^+, 11), 164 (9), 163 (100), 134 (45), 92 (10), 91 (14). Anal. ($C_{16}H_{18}N_2O_3S$) C, H, N.

1-(4-Methoxyphenyl)diazoethane (22). Preparation of the diazo compound in the usual manner produced a substantial amount of *p*-methoxystyrene (**24**) as a contaminant. IR (Ar, 15 K) 2055 s, 1272 s, 1188 s, 1082 w, 1049 s, 823 s, 805 m, 673 w, 614 m, 524 m, 482 w cm^{-1}. The deep-red diazo compound was sublimed at 0 °C (10^{-6} Torr) and codeposited with argon to form a matrix.

1-Diazo-1-phenyl-2-propanone (21) was prepared by the method of Regitz:[61] IR (Ar, 15 K) 2098 m, 2070 vs, 1679 s, 1660 w, 1611 w, 1503 m, 1369 s, 1331 m, 1290 m, 1245 s, 1148 w, 1036 m, 1008 w, 908 m, 752 s, 691 m, 618 m, 494 w cm^{-1}. The sample was sublimed at 8 °C (10^{-6} Torr) and codeposited with argon to form a matrix.

Acknowledgment. We gratefully acknowledge the financial support of the National Science Foundation (Grant CHE84-04949) and the National Institutes of Health (Grant GM-24427). The National Science Foundation (1980-1983) and the IBM Corporation (1983-1984) provided predoctoral fellowships (R. J.M.). The National Science Foundation, the National Institutes of Health, the IBM Corp., and the Mobil Corp. supplied funds for the purchase of the Nicolet 60SX FTIR spectrometer.

Registry No. 12a, 698-20-4; **12b**, 105930-64-1; **13a**, 35745-45-0; **16a**, 22293-10-3; **16b**, 105930-66-3; **17a**, 6393-09-5; **21**, 3893-35-4; **22**, 70078-14-7; D_2, 7782-39-0; *o*-tolualdehyde tosylhydrazone, 35629-84-6; *o*-(trideuteriomethyl)benzaldehyde, 77765-22-1; *o*-(trideuteriomethyl)-benzaldehyde tosylhydrazone, 105930-63-0; α,α,α-trideuterioacetophenone tosylhydrazone, 105930-65-2; *p*-methoxyacetophenone tosylhydrazone, 32117-52-5; *o*-bromobenzaldehyde, 6630-33-7; acetophenone tosylhydrazone, 4545-21-5.

σ and π Interactions of the Carbonyl Ligand Determined from Single-Crystal Polarized Electronic Spectroscopy and Ligand Field Theory

Tsu-Hsin Chang and Jeffrey I. Zink*

Contribution from the Department of Chemistry and Biochemistry, University of California, Los Angeles, Los Angeles, California 90024. *Received August 18, 1986*

Abstract: The single-crystal polarized electronic absorption spectra of $(Pr_4N)[PtCl_3CO]$, $(Pr_4N)[PtBr_3CO]$, and $(Pr_4N)[PtCl_3CNC(CH_3)_3]$ taken at 10 K are reported. Spin-allowed and spin-forbidden ligand field (d-d) transitions and charge-transfer transitions are assigned. The σ and π interactions of the carbonyl ligand with the metal d orbitals are obtained from full-matrix angular overlap ligand field theory calculations including spin-orbit coupling. The AOM σ and π parameters show that carbon monoxide is a very strong π acceptor ligand and that it is a good σ donor ligand. The σ and π interaction parameters are compared to those of other ligands of interest in organometallic chemistry, and the position of the carbonyl ligand in the two-dimensional spectrochemical series is reported. These comparisons show that carbon monoxide is a better σ donor ligand than the chloride ion and about equal to ethylene. The properties of the isonitrile ligand are similar to those of the carbonyl ligand. Bond length changes in excited electronic states determined from Franck-Condon analysis of the vibronic structure are reported.

The relative σ and π bonding properties of carbon monoxide in transition-metal complexes have been the subject of many experimental and theoretical studies. The importance of π back-bonding is firmly embedded in inorganic lore and is well documented in standard textbooks.[1] The σ-bonding properties, however, are not well documented.

The experimental measurement which is most amenable to theoretical interpretation and which has yielded the most insight into the bonding properties is IR spectroscopy. The standard lists of π-acceptor ligand series have been determined from trends in the CO stretching frequencies or from Cotton-Kraihanzel force constants.[1,2] Extensions of this type of analysis have led to the development of series based on both σ and π effects.[3] The general conclusion is that carbon monoxide is one of the best π-acceptor ligands but a poor σ donor. Other researchers have argued that there has been an overemphasis on π effects and that both σ and π interactions must be considered.[4,5]

Another experimental method of determining σ and π interactions of ligands with transition metals is electronic absorption spectroscopy. The σ and π interactions can be determined from transition energies and interpreted by using the angular overlap theory.[6] However, such studies have been inhibited by three factors. First, the d-d transitions in complexes containing the carbonyl ligand are usually high in energy (as expected from a strong π-acceptor ligand). Second, intense charge-transfer bands, often in the same energy region as the d-d bands, obscure the weaker d-d bands which are needed for the analysis. Finally, the extinction coefficients are frequently large, thus preventing single-crystal polarized absorption spectra and hence resolved absorption bands from being obtained. A series of compounds in which the above problems can be overcome is the $PtCl_3L^-$ series where L can range from Werner ligands[7-15] to olefins,[16] phosphines,

(1) Cotton, F. A.; Wilkinson, G. W. *Advanced Inorganic Chemistry*, 4th ed.; Wiley: New York, 1980; p 1078. Huheey, J. E. *Inorganic Chemistry*, 3rd ed.; Harper and Row: Cambridge, 1983; pp 432-441. Purcell, K.; Kotz, J. c. *Inorganic Chemistry*, Saunders, Philadelphia, 1977; p 201.
(2) Cotton, F. A.; Kraihanzel, C. S. *J. Am. Chem. Soc.* **1962**, *84*, 4432.
(3) Graham, W. A. G. *Inorg. Chem.* **1968**, *7*, 315.
(4) Angelici, R. J.; Ingemanson, C. M. *Inorg. Chem.* **1969**, *8*, 83.
(5) Brown, T. L.; Darensbourg, D. J. *Inorg. Chem.* **1968**, *7*, 959.
(6) Schaffer, C. E.; Jorgensen, C. K. *Mol. Phys.* **1965**, *9*, 401. Schaffer, C. E. *Struct. Bonding* **1968**, *5*, 68.
(7) Fenske, R. F.; Martin, D. S.; Ruedenberg, K. *Inorg. Chem.* **1962**, *1*, 441.

0002-7863/87/1509-0692$01.50/0

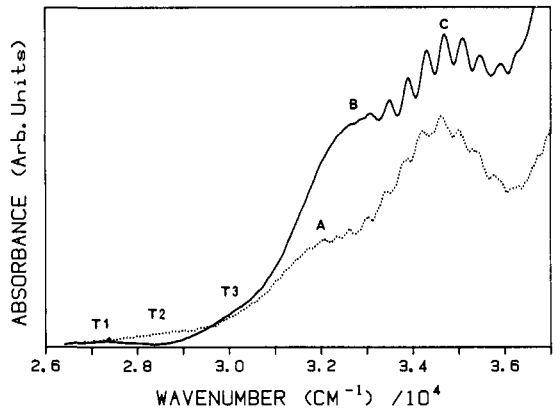

Figure 1. Single-crystal polarized electronic absorption spectra of $(Pr_4N)[PtCl_3CO]$ at 10 K. Dotted line, parallel polarization. Solid line, perpendicular polarization.

and arsines.[17,18] New microspectroscopic techniques allow polarized electronic spectra to be obtained from crystals even when $\epsilon > 10^3$ L/(M·cm).[16,19] Only the ligand L is changed in the series. Hence the systematic changes in the σ and π properties of the ligand L can be interpreted from the electronic spectra.

We report here electronic spectroscopic results for $PtCl_3CO^-$ and $PtBr_3CO^-$ and for comparison those of $PtCl_3CNC(CH_3)_3^-$. The single-crystal polarized electronic absorption spectra at 10 K, the luminescence of the carbonyl complex, the assignments of the bands, and the angular overlap σ and π parameters are reported. The geometry changes in excited states are determined from the well-resolved vibronic structure. The σ and π interactions of the carbonyl ligand are compared to those of other ligands of organometallic interest, and the position of the carbonyl ligand in the two-dimensional spectrochemical series is determined for the first time.

Experimental Section

The compounds $(Pr_4N)[PtCl_3CO]$, $(Pr_4N)[PtBr_3CO]$, and $(Pr_4N)[PtCl_3CNC(CH_3)_3]$ were prepared by reacting the dimer $(Pr_4N)_2[Pt_2X_6]$, X = Cl^- or Br^-, with CO or $CNC(CH_3)_3$.[20-22] The single crystals for spectroscopic measurements of all of the compounds were grown between quartz plates from a dichloromethane solution. A drop of the solution was placed on one plate and a second plate was pressed over the first. The plates were stored in the dark. After several hours, crystals having dimensions on the order of 100 × 100 × 0.1 μm were obtained.

The spectra of $(Pr_4N)[PtCl_3CO]$ were obtained from crystal faces which have the extinction axis about 12° from the long crystal axes. The spectra of $(Pr_4N)[PtBr_3CO]$ were obtained from crystal faces with the extinction axis at an angle of 7° to the long crystal axis. The spectra of $(Pr_4N)[PtCl_3CNC(CH_3)_3]$ were obtained from three different types of crystals. Two types, with extinction axes at angles of 18° and 34° from one of the crystal axes, respectively, were grown from CH_2Cl_2. The third type, which grew in long rectangles with an extinction axis at an angle of 5° from the long axis, was grown from acetone. Because of the microscopic dimensions of the crystals it is not known if the three types of observed properties arise from different crystal faces or different polymorphs. The spectra from all of the crystals were obtained with the electric vector of the incident radiation parallel to and orthogonal to the above extinction axes.

The instrument which was used to obtain the crystal spectra is a locally constructed microspectrophotometer which has been described previously.[16] The solution-phase spectra were recorded by using a Cary 14 spectrophotometer.

Table I. Peak Maxima and Assignments

absorption max, cm^{-1}	assignment	label in Figures 1, 2, or 3
	$(Pr_4N)[PtCl_3CO]$	
27 000	triplet	T1
28 500	triplet	T2
30 000	triplet	T3
31 900	$^1A_2\ d_{yz} \rightarrow d_{x^2-y^2}$	A
32 600	$^1B_1\ d_{xy} \rightarrow d_{x^2-y^2}$	B
34 700	$^1B_2\ d_{xz} \rightarrow d_{x^2-y^2}$	C
	$(Pr_4N)[PtBr_3CO]$	
25 000[a]	triplet	T1
28 000	triplet	T2
29 800	$^1A_2\ d_{yz} \rightarrow d_{x^2-y^2}$	A
30 800	$^1B_1\ d_{xy} \rightarrow d_{x^2-y^2}$	B
32 800	$^1B_2\ d_{xz} \rightarrow d_{x^2-y^2}$	C
34 400	LMCT Br → Pt	D
	$(Pr_4N)[PtCl_3(CNC(CH_3)_3)]$	
20 800	triplet	T1
24 500	triplet	T2
27 000	triplet	T3
30 900[b]	$^1A_2\ d_{yz} \rightarrow d_{x^2-y^2}$	A
31 800[b]	$^1B_1\ d_{xy} \rightarrow d_{x^2-y^2}$	B
34 000[b]	$^1B_2\ d_{xz} \rightarrow d_{x^2-y^2}$	C

[a] Very broad extending from about 24 000 to 26 000 cm^{-1}. [b] Very poorly resolved shoulder.

Results

The electronic absorption spectra at 10 K of a single crystal of $(Pr_4N)[PtCl_3CO]$ are shown in Figure 1. The spectrum labeled "parallel" was taken with the electric vector of the incident radiation parallel to the extinction direction at an angle of 6.4° to the long axis of the crystal. The perpendicular spectrum was obtained in the orthogonal extinction direction. The projection of the electric vector of the incident radiation on the molecular axes cannot be determined in this experiment because of the microscopic size of the crystals required to obtain the absorption spectra and because the crystal structure is not known. The observed polarization changes provide a very useful method for resolving closely spaced features. The energies of the peaks and shoulders are given in Table I and are labeled as shown in Figure 1.

Three broad overlapping bands labeled T1 through T3 are observed in the low-energy region of the spectrum shown in Figure 1. Band T1 at about 27 000 cm^{-1} is observed in both polarization directions. Band T2 at about 28 500 cm^{-1} is polarized primarily in the parallel polarization direction while band T3 at about 30 000 cm^{-1} is most prominent in the perpendicular polarization direction.

Three bands labeled A, B, and C are observed in the high-energy region of the spectrum. Band A is more intense in the parallel polarization direction. It shows weak vibronic structure. Band B is most readily observed in the perpendicular polarization direction. Its maximum is almost resolved. The most intense feature, band C at 34 700 cm^{-1}, is completely resolved. It is observed in both polarizations but is more intense in the perpendicular polarization direction. It shows well-developed vibronic progressions.

The positions of the vibronic peaks observed on bands A and C are given in Table II. The four clearly discernable vibronic peaks on band A have an average spacing of 290 cm^{-1}. The eight peaks observed in the parallel polarization on band C have an average spacing of 402 cm^{-1}, and the nine peaks observed in the perpendicular polarization have an average spacing of 401 cm^{-1}. The vibronic peaks in the two different polarization directions are offset from each other by about 80 cm^{-1}. The ground-state metal–ligand normal modes and their frequencies are the following:

(8) (a) Kroening, R. F.; Rush, R. M.; Martin, D. S.; Clardy, J. C. *Inorg. Chem.* **1974**, *13*, 1366. (b) Martin, D. S.; Tucker, M. A.; Kassman, A. J. *Inorg. Chem.* **1965**, *4*, 1682.
(9) Fanwick, P. E.; Martin, D. S. *Inorg. Chem.* **1973**, *12*, 24.
(10) Martin, D. S. *Inorg. Chim. Acta Rev.* **1971**, *5*, 107.
(11) Patterson, H. H.; Godfrey, J. J.; Khan, S. M. *Inorg. Chem.* **1972**, *11*, 2872.
(12) Francke, E.; Moncuit, C. *Theor. Chim. Acta* **1973**, *29*, 319.
(13) Tuszynski, W.; Gliemann, G. *Z. Naturforsch. A* **1979**, *34A*, 211.
(14) Van Quickenborne, L. G.; Ceulemans, A. *Inorg. Chem.* **1981**, *20*, 796.
(15) Chang, T.-H.; Zink, J. I. *Inorg. Chem.* **1985**, *24*, 4499.
(16) Chang, T.-H.; Zink, J. I. *J. Am. Chem. Soc.* **1984**, *106*, 287.
(17) Phillips, J.; Zink, J. I. *Inorg. Chem.* **1986**, *25*, 1503.
(18) Chang, T.-H.; Zink, J. I. *Inorg. Chem.* **1986**, *25*, 2736.
(19) Chang, T.-H.; Zink, J. I. *Inorg. Chem.* **1985**, *24*, 4016.
(20) Goodfellow, R. J.; Venanzi, L. M. *J. Chem. Soc.* **1965**, 7533.
(21) Goodfellow, R. J.; Goggin, P. L.; Venanzi, L. M. *J. Chem. Soc. A* **1967**, 1892.
(22) Goggin, P. L.; Goodfellow, R. J. *J. Chem. Soc., Dalton Trans.* **1977**, 2061.

Table II. Energies of the Vibronic Bands in the Electronic Spectrum of $[Pr_4N][PtCl_3(CO)]$

electronic band	max (cm^{-1})	separation (cm^{-1})
$^1B_2$ (∥)	32589	
	32996	407
	33394	398
	33794	400
	34201	407
	34608	407
	35003	395
	35404	401
		av 402
$^1B_2$ (⊥)	33077	
	33481	404
	33885	404
	34277	392
	34681	404
	35085	404
	35491	406
	35895	404
	36285	390
		av 401
$^1A_2$	31742	
	32042	300
	32337	295
	32611	274
		av 290

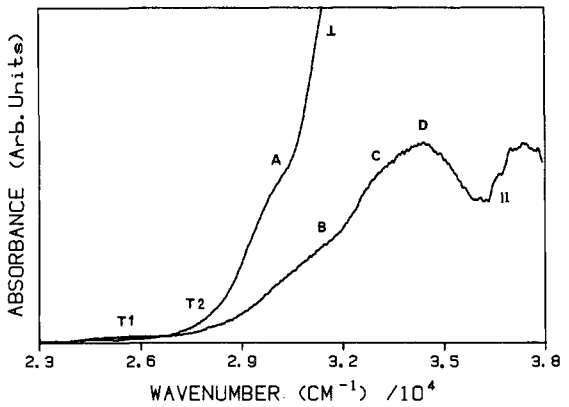

Figure 2. Single-crystal polarized electronic absorption spectra of $(Pr_4N)[PtBr_3CO]$ at 10 K.

metal–carbon stretch, 507 cm^{-1}, platinum–chloride (cis) stretch, 324 cm^{-1}; and platinum–chloride (trans) stretch, 348 cm^{-1}.[22] The vibronic structure will be discussed later.

Weak luminescence is observed when the compound is excited at low temperature by the 457.9-nm line or the UV lines of an Ar^+ laser. The broad emission peak has its maximum at 16500 cm^{-1} and its origin at about 21000 cm^{-1}. Because of the low intensity and the poor signal-to-noise ratio, no further analysis of the luminescence was attempted.

The electronic absorption spectra at 10 K of single crystals of $(Pr_4N)[PtBr_3CO]$ are shown in Figure 2. The spectrum labeled "parallel" was obtained with the electric vector of the incident radiation parallel to the extinction direction at an angle of 6.6° to the long crystal axis. The perpendicular spectrum was obtained in the orthogonal extinction direction. The crystal structure has not been determined. The two polarization directions are again used to resolve various spectral features and cannot be related to specific molecular axes. The energies of the bands are given in Table I.

A very intense band at about 34500 cm^{-1} which is allowed in the perpendicular direction obscures most of the features in that spectrum. In the parallel polarization direction, this band is drastically diminished in intensity and features analogous to those in the spectrum of $PtCl_3CO^-$ are observed. The 34500-cm^{-1} band, labeled band D, is not completely extinguished and its maximum can be seen in the parallel spectrum.

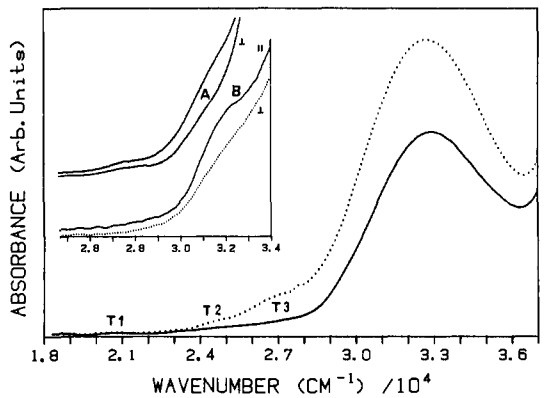

Figure 3. Single-crystal polarized electronic absorption spectra of $(Pr_4N)[PtCl_3CNC(CH_3)_3]$ at 10 K. Spectra I, II, and III are taken from three different crystal faces.

In the low-energy region of the spectrum at least two weak bands are observed at about 25000 and 28000 cm^{-1}. They are labeled T1 and T2, respectively. These weak bands are not very pronounced because the crystal is extremely thin.

Three shoulders are observed to higher energy. These shoulders, labeled A, B, and C, are analagous to the three features with the same labels in the spectrum of $PtCl_3CO^-$ but are shifted about 1900 cm^{-1} to the red. The energies of these features cannot be determined as accurately because they are not as well resolved. The approximate energies are listed in Table I.

A feature at the high-energy side of the spectrum, labeled band E, is observed at about 37500 cm^{-1}. This band has no counterpart in the spectrum of $PtCl_3CO^-$. It contains poorly resolved but clearly discernable vibronic structure. Band E occurs at the high-energy limit of our instrument where instrumental errors become large. Thus the energy of this electronic transition cannot be determined with certainty.

The electronic absorption spectra at 10 K of three different single crystals of $(Pr_4N)[PtCl_3(CNC(CH_3)_3]$ are shown in Figure 3. The spectra shown in the insert were taken from crystals grown from dichloromethane solutions. These crystals were rhombic. The extinction axes lie at angles of 34.4° and 18° to one of the crystal axes. A third type of crystal was grown from acetone. It is rectangular with an extintion direction at an angle of 5.3° to the long crystal axis. The crystal structure is not known. Hence the extinction directions cannot be related to molecular axes and the polarization experiments are used to help determine the positions of the closely spaced absorption bands.

The spectrum of $PtCl_3(CNC(CH_3)_3)^-$ consists of a series of closely spaced overlapping bands. From the composite spectra in Figure 3 from the three different faces of the two different crystal forms, the positions of most of the bands can be approximately determined. Three weak features on the low-energy side of the spectra, labeled T1 through T3, are observed. On the high-energy side of the spectra, at least three features are observed. Two of them, labeled A and B, appear as shoulders at about 30900 and 31800 cm^{-1}, respectively. Shoulder A is most clearly seen in the upper spectrum in the insert while shoulder B is almost resolved in the lower spectrum in the insert. In the main spectrum shown in Figure 3 an asymmetric peak is observed at about 33000 cm^{-1}. This apparent peak is probably the sum of two bands, band B and a new band C which is located at about 34000 cm^{-1}. The severe overlapping of bands A, B, and C will make a detailed analysis impossible. Note, however, that the pattern of these bands is the same as that observed in $PtCl_3CO^-$ and that each of these bands is shifted about 900 cm^{-1} to the red of the analagous band in the spectrum of $PtCl_3CO^-$.

Discussion

Assignments. The bands in the electronic absorption spectra of the three compounds discussed here are categorized and assigned in three groups: spin-forbidden (triplet) ligand field transitions, spin-allowed (singlet) ligand field transitions, and charge-transfer

transitions. The general patterns of the spectra are very similar to those in the spectra of the other $PtCl_3L$ complexes which have been studied in our laboratory to date. This pattern consists of two or three low-intensity ($\epsilon < 100$) bands at the low-energy end of the spectrum, three medium-intensity ($100 < \epsilon < 1000$) bands in the middle of the spectrum, and finally high-intensity bands ($\epsilon > 10^3$) at the high-energy side of the spectrum. Because of the similarities, the ligand field bands are assigned in a manner consistent with the assignments of the earlier spectra. The axis system which is used in all of these assignments has the z axis perpendicular to the square plane and the x axis along the unique ligand–metal bond. The B_1 irreducible representation is defined as the one symmetric to reflection in the xy mirror plane.

The absorption spectrum of $(Pr_4N)[PtCl_3CO]$ is very similar to that of Zeise's salt, $K[PtCl_3C_2H_4]$ in the spin-allowed region.[16] In both complexes, a strong allowed peak in one polarization (band B in Figure 1), a weak shoulder in a different polarization (band A), and another strong peak which is observed in both polarizations (band C) are observed. In the solution spectrum of $(Pr_4N)[PtCl_3CO]$ in CH_2Cl_2, bands at 32 600 and 35 700 cm^{-1} with molar absorptivities of 460 L/(M·cm) and 690 L/(M·cm), respectively, are observed. The molar absorptivities of these bands are in the range of those for spin-allowed d–d transitions in square-planar platinum complexes. Following the reasoning used in previous assignments, band B is assigned to the $^1A_1 \rightarrow {}^1B_1$, $d_{xy} \rightarrow d_{x^2-y^2}$ transition, the dipole forbidden vibronically allowed band A is assigned to the $^1A_1 \rightarrow {}^1A_2$, $d_{yz} \rightarrow d_{x^2-y^2}$ transition, and band C is assigned to the $^1A_1 \rightarrow {}^1B_2$, $d_{xz} \rightarrow d_{x^2-y^2}$ transition.

The bands to lower energy (bands T1–T3) are assigned to transitions to triplet excited states. The molar absorptivity observed in the solution spectrum band at 23 500 cm^{-1} is 44 L/(M·cm). These bands are assigned primarily by using ligand field theory. They can never be readily assigned solely from their polarization properties, even when full crystallographic data are known, because their intensities are very sensitive to their couplings to singlet states. The calculations, including spin–orbit coupling, show that the observed maxima are actually a superposition of clusters of closely spaced spin–orbit coupled components of the triplet states. The assignments of bands T1–T3 are discussed below in conjunction with the ligand field calculation.

In the solution spectrum, a band at 39 500 cm^{-1} with a molar absorptivity of 3650 L/(M·cm) is observed. This band is tentatively assigned to the platinum to carbonyl spin-forbidden charge-transfer transition. It is probably not the chloride-to-platinum charge-transfer transition because its energy is much lower than that of the corresponding charge-transfer band observed at 45 300 cm^{-1} in $PtCl_3NH_3^-$.[9] The 39 500-cm^{-1} band obscures the region where the d_{z^2} to $d_{x^2-y^2}$ transition is calculated to occur.

The assignments of the bands in the spectra of $(Pr_4N)[PtBr_3CO]$ are very similar to those in the chloro derivative discussed above. Martin et al. observed that there is a fairly uniform red shift of about 2000 cm^{-1} between the singlet d–d transition energies in $PtCl_4^{2-}$ and $PtBr_4^{2-}$.[8] The bands in the $PtBr_3CO^-$ complex are shifted by about 2000 cm^{-1} to the red relative to the analogous bands in the chloro complex. The major difference between the spectra is the presence of band D at 34 400 cm^{-1} in the spectrum of $PtBr_3CO^-$ which is absent in the spectrum of the chloro complex. This band is tentatively assigned to the bromo-to-platinum charge-transfer transition. In the solution spectrum, a band at 34 800 cm^{-1} with a molar absorptivity of 3510 L/(M·cm) is observed, consistent with a charge-transfer transition. The spectrum of K_2PtBr_4 showed a band at 34 200 cm^{-1} which has been assigned to a bromide-to-platinum charge transfer mixed with a platinum-to-bromide charge transfer.[8] The similarity of the energies supports the assignment.

The single-crystal polarized absorption spectra of $(Pr_4N)[PtCl_3CNC(CH_3)_3]$ are so poorly resolved that assignment of the bands becomes speculative. The procedure is somewhat aided by the common bands which are found in the spectra from three different crystal's faces and/or polymorphs. The weak and broad features labeled T1–T3 found in the low-energy region of the spectra are assigned to transitions to triplet excited states. At least three features can be identified on the high-energy side. Two of them are the shoulders A and B. In the main spectrum, an asymmetric peak is observed at about 33 000 cm^{-1} which is probably the sum of two bands, band B and a new band C which has its peak to slightly higher energy. In the solution spectrum in acetonitrile, bands are observed at energies (cm^{-1}) of 22 500 ($\epsilon = 26$), 27 500 ($\epsilon = 62$), 31 500 ($\epsilon = 140$) and 39 200 ($\epsilon = 960$). Bands A, B, and C can thus be tentatively associated with the spin-allowed ligand-field transitions. Note that each of these bands is shifted to the red of the analogous bands in $PtCl_3CO^-$ by about 900 cm^{-1}. Because of the severe overlapping, no detailed analysis will be carried out.

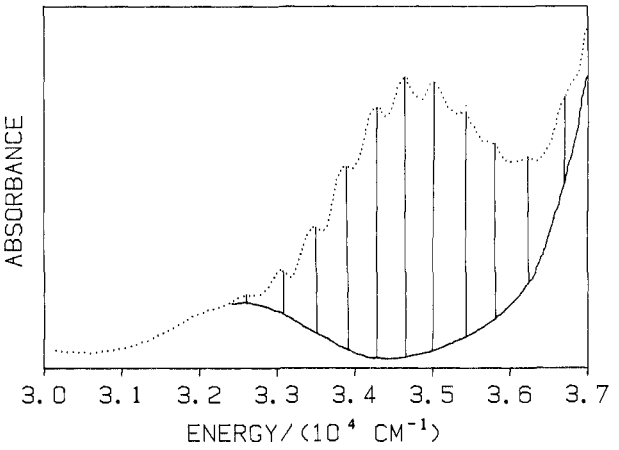

Figure 4. Vibronic structure on the $^1B_2$ absorption band of $(Pr_4N)[PtCl_3CO]$ at 10 K. The vertical bars are the intensities calculated by using a metal–carbon distortion of 0.18 Å.

Vibronic Structure. Well-defined vibronic structure is observed on the $^1B_1$ band (band C in Figure 1) of the spectrum of $(Pr_4N)[PtCl_3CO]$. The structure is better resolved in the spectrum taken by using perpendicular polarization than it is in the spectrum obtained by using parallel polarization. However, in the parallel spectrum the overlap of the other bands with the $^1B_1$ band is not as severe and the relative intensities of the members of the progression are more readily obtained. The average spacing between the vibronic bands in both polarizations is 402 cm^{-1}. This spacing, which represents the excited-state Pt–CO vibrational frequency, is reduced by about 100 cm^{-1} from the ground-state Pt–CO stretching frequency of 507 cm^{-1}.[22]

The $^1A_2$ band contains poorly resolved vibronic structure. The average spacing of 290 cm^{-1} between four members can be determined from the derivative spectrum. This vibrational frequency is associated with either the cis Pt–Cl stretch with a ground-state frequency of 324 cm^{-1} or the trans Pt–Cl stretch with a frequency of 348 cm^{-1}.[22]

The coupling of the Pt–CO vibration with the $^1A_1$ to $^1B_2$ transition can be explained in terms of the orbital properties of the transition. This transition corresponds to a one-electron promotion from the d_{xz} orbital to the $d_{x^2-y^2}$ orbital. The d_{xz} orbital participates in π bonding between the Pt and C while the $d_{x^2-y^2}$ orbital participates in σ bonding between these atoms. Thus the transition weakens both the π bonding and the σ bonding between the metal and the carbon. This weakening leads to a large displacement of the potential surface along the totally symmetric Pt–C stretching normal model relative to the ground electronic state and thus a large Franck–Condon progression in that mode.

The magnitude of the bond lengthening in the excited state can be calculated from the Franck–Condon factors. The calculational procedure has been discussed previously.[23] In the case of the $^1B_1$ band, the accuracy of the calculation is limited because both the $^1B_1$ band on the low-energy side and the edge of the charge-transfer band on the high-energy side overlap the structured band. The vibronic intensities calculated by using the ground- and excited-

(23) Yersin, H.; Otto, H.; Zink, J. I.; Gliemann, G. *J. Am. Chem. Soc.* **1980**, *102*, 951.

Table III. Trends in Experimentally Measured Energies

unique ligand	$^1A_2$ energy	$^1B_2 - {}^1A_2$ energy difference
PEt_3[a]	36 200	−500
NMe_3[b]	350	−2140
PPh_3[c]	33 400	1910
$AsPh_3$[c]	33 458	2040
C_2H_4[d]	30 350	2450
CO[e]	31 900	2800
$CNC(CH_3)_3$[e]	30 900	3100
Cl^-[f]	29 200	0

[a] Reference 17. [b] Reference 15. [c] Reference 18. [d] Reference 16. [e] This work. [f] References 12 and 14.

state frequencies, a spectral origin of 32 589 cm^{-1} (Table II), and a distortion of 0.175 Å are shown superimposed on the experimental spectrum in Figure 4. The uncertainty in the height of the base line produces an uncertainty of about ±0.02 Å in the determination of the distortion.

The change of the Pt–C bond length of about 0.18 Å from its ground-state value of 1.82 Å[24] is typical for metal–CO bonds.[25] The sign of the distortion cannot be obtained from the calculation, but the bonding properties of the orbitals involved in the transition strongly suggest that the bond is lengthened in the excited state. The large lengthening is consistent with the observed 100-cm^{-1} decrease in the stretching frequency.

Calculation of the Transition Energies and the Ligand-Field Parameters. The transition energies are treated by the angular overlap model (AOM) in terms of parameters representing the σ and π interactions between the metal and the ligands. For example, the energy of the $d_{x^2-y^2}$ orbital will depend on its σ interactions with the chloride ligands, e_σ^{Cl}, and the σ interaction with the carbonyl e_σ^{CO}. Correspondingly, the d_{xy} orbital energy will depend on the in-plane π interactions with these ligands, e_π^{Cl} and e_π^{CO}. The state energies are calculated from the one-electron orbital energies by using the symmetry-adapted wave functions and evaluating the matrix elements. The electron repulsion energies are expressed in terms of the Racah parameters B and C. The matrix elements have been tabulated and will not be repeated here.[12] Finally, the transition energies are calculated by diagonalizing the complete energy matrix and calculating the energy differences between the ground state and the various excited states.

Two methods of treating the spectra of the $PtCl_3L^-$ compounds will be discussed. The most complete method is the full-matrix calculation, including spin–orbit coupling, of the transition energies as a function of the ligand-field parameters. The results of this calculation are discussed later. First, only the diagonal elements are examined. A great deal of physical insight into the meaning of the transition energies can be obtained from this simplified method. In addition, a rough estimate of the trends in the metal–ligand interactions in a series of $PtCl_3L^-$ complexes as a function of the trends in the spectra can be obtained by using this simplified method although accurate values of the parameters cannot be calculated.

The three lowest singlet d–d transition energies in terms of the diagonal elements are given by

$$\Delta E(^1B_1) = -C + 3/4(3e_\sigma^X + e_\sigma^L) - 3e_\sigma^X - e_\pi^L \quad (1)$$

$$\Delta E(^1A_2) = -3B - C + 3/4(3e_\sigma^X + e_\sigma^L) - 2e_\pi^X \quad (2)$$

$$\Delta E(^1B_2) = -3B - C + 3/4(3e_\sigma^X + e_\sigma^L) - e_\pi^X - e_\pi^L \quad (3)$$

where B and C are the Racah parameters, e_π^X and e_σ^L are the AOM σ parameters, and e_π^X and e_p^L are the π parameters for the halide X and the unique ligand L. For simplicity the equations are written in the form for $e_{\pi,\parallel} = e_{\pi,\perp}$. Two quantities which can be obtained directly from the experimental spectrum are important to the qualitative interpretation: the energy of the $^1A_2$ transition, eq 2, and the energy difference between the $^1B_2$ and the $^1A_2$ states, eq 4. The trend in the σ donor ability of the ligand L can be

$$\Delta E(^1B_2) - \Delta E(^1A_2) = e\pi^X - e_\pi^L \quad (4)$$

experimentally determined from the trend in the energy of the $^1A_2$ state. The trend in this energy, given in eq 2, is dominated by the trend in e_σ^L because the energy contribution from the Racah parameters only varies by several 10^2 cm^{-1} from compound to compound, and the parameters from the chloride ligand are roughly constant from compound to compound in the $PtCl_3L^{n-}$ series (vide infra). The $^1A_2$ transition energies for complexes of the ligands L discussed above are listed in Table III. The trend in the σ donor ability of the ligands increases in the order $Cl < C_2H_4 < CNC(CH_3)_3 < CO < AsPh_3 < PPh_3 < NMe_3$.

The trend in the π interactions between the ligand L and platinum can be determined from the trend in the $^1B_2 - {}^1A_2$ energy separation in the experimental spectrum. This energy difference, according to eq 4, varies with e_π^L as the ligand L is changed. The contribution from e_π^{Cl} is roughly constant from compound to compound. The experimentally determined energy separation is given in Table III for the ligands discussed above. The smaller the value of e_π^L, the larger the π acceptor ability of the ligand. Thus the trend in π acceptor ability, ordered from smallest to largest, is $NMe_3 < PEt_3 < Cl < PPh_3 < AsPh_3 < C_2H_4 < CO < CNC(CH_3)_3$. The orderings obtained above are those expected from chemical intuition with one exception: chloride appears to be a poorer π donor than expected. This result could be caused by some π-acceptor interaction between empty π orbitals on Cl with the high-energy 5d orbitals on platinum. Alternatively, the ligand L might have large electrostatic interactions with the radially large platinum 5d orbitals which raise the 5d orbital energies and make the ligands appear to be better π donors, i.e., poorer π acceptors. The latter possibility is discussed below in conjunction with the matrix calculation of the AOM parameters.

Table IV. Calculated and Observed Transition Energies for $(Pr_4N)[PtCl_3CO]$[a]

calculated	observed	assignment	label
singlets			
32 125	31 900	$^1A_2$	A
32 584	32 600	$^1B_1$	B
34 588	34 700	$^1B_2$	C
35 870[b]		$^1A_1$	
triplets			
23 085		B_1	
23 095		B_2	
23 313		A_1	
26 687		A_2	
26 795	27 000	B_1	T1
26 916		A_2	
27 875		A_1	
28 474	28 500	B_2	T2
30 875		B_2	
31 268	30 000	B_1	T3
31 304		A_2	
31 557		A_1	

[a] The transition energies were calculated by using the following parameters (cm^{-1}): $e_\sigma^{Cl} = 11\,800$, $e_{\pi\parallel}^{Cl} = 2400$, $e_{\pi\perp}^{Cl} = 3400$, $e_\sigma^{CO} = 14\,500$, $e_{\pi\parallel}^{CO} = -2200$, $e_{\pi\perp}^{CO} = -1300$, $\sigma_{sd} = 12\,475$, $B = 550$, $C = 750$, $\xi = 2200$. The π parameters have in-plane ($\parallel$) and out-of-plane ($\perp$) components; the mean value is discussed in the text. [b] The calculated energy includes s–d mixing.

AOM Energy Matrix Calculations. The singlet and triplet transition energies for the $PtCl_3CO^-$ complexes which are calculated by diagonalizing the AOM energy matrix are given in Table IV. The AOM parameters which were used are included in the tables. The same assumptions as those discussed and used in previous work were employed in these calculations, i.e., the chloride parameters and the spin–orbit coupling constant were assumed to be transferrable from complex to complex within the narrow range of several hundred wavenumbers.

(24) Russell, D. R.; Tucker, P. A.; Wilson, S. *J. Organomet. Chem.* **1976**, *104*, 387.
(25) Trogler, W. C.; Desjarding, S. R.; Solomon, E. I. *Inorg. Chem.* **1979**, *18*, 2131.

Table V. Calculated and Observed Transition Energies for $(Pr_4N)[PtBr_3CO]$[a]

calculated	observed	assignment	label
singlets			
29 962	29 800	$^1A_2$	A
30 898	30 800	$^1B_1$	B
32 525	32 800	$^1B_2$	C
33 540	*b*	$^1A_1$	
triplets			
21 203		B_1	
21 209		B_2	
21 497		A_1	
24 200		A_2	
24 338		B_1	
25 103	24 000–26 000	A_2	T1
25 635		A_1	
25 969		B_2	
28 818		B_1	
29 153	28 000	B_2	T2
29 592		A_2	
29 897		A_1	

[a] The transition energies were calculated by using the following parameters (cm^{-1}): e_σ^{Br} = 10 830, $e_{\pi\parallel}^{Br}$ = 2190, $e_{\pi\perp}^{Br}$ = 3000, e_σ^{CO} = 14 500, $e_{\pi\perp}^{CO}$ = −2100, $e_{\pi\parallel}^{CO}$ = −1200, σ_{sd} = 11 747, B = 600, C = 750, ξ = 2200. [b] Obscured by the Br to Pt charge-transfer band. The calculated energy includes s–d mixing.

The quantitative agreement between the calculated and observed singlet state transition energies is very good. The mean discrepancy between the measured and calculated singlet state transition energies is 120 cm^{-1}. The calculations also are in agreement with the assignments made in the previous section.

The calculated transition energies of the triplet states also agree well with the observed transitions. The calculation, including spin–orbit coupling, shows that the observed bands do not arise from a single "triplet" state such as $^3A_2$, but instead they are composed of clusters of spin–orbit coupled components. These results illustrate why polarization properties alone cannot be used to assign these states. The intensities depend strongly on the amount of singlet character which is mixed into each component. The energies of calculated spin–orbit states and their symmetries are given in Table III.

The transition energies for $(Pr_4N)[PtBr_3CO]$ complex which are calculated by diagonalizing the AOM energy matrix are given in Table V. The AOM parameters which are used in the calculation are given at the bottom of the table. The agreement between the calculated and observed singlet-state transition energies is very good. The mean discrepancy between the measured and calculated energies is 180 cm^{-1}. Because the peak separations are not as well defined in the spectrum of this complex as they are in that of $(Pr_4N)[PtCl_3CO]$, the values of the parameters are not as accurately determined.

The peaks in the experimental spectrum of $(Pr_4N)[PtCl_3CNC(CH_3)_3]$ are the most poorly separated of those in the compounds studied in this work. Because of the increased uncertainties in the energies of the peak maxima, no attempt was made to refine the best fit AOM parameters. By using the same parameters as those used for the $PtCl_3CO^-$ complex and e_σ^C = 13 000 cm^{-1}, $e_{\pi,\parallel}^C$ = −2200 cm^{-1}, and $e_{\pi,\perp}^C$ = −1300 cm^{-1}, a reasonable fit (mean discrepancy between the calculated and observed singlet transition energies = 320 cm^{-1}) was obtained. The uncertainty limits on the values of the σ and π parameters for the isonitrile ligand are larger than those for the parameters of the other ligands which have been studied in the $PtCl_3L$ series which are discussed below.

Transferability of the Parameters between Complexes. An important aspect of the AOM σ and π parameters which must be kept in mind when comparing the values for a series of ligands is their expected variability from compound to compound. A common assumption, which has been shown to hold quite well for ionic compounds, is that the AOM parameters for a given ligand are almost constant and can be transferred in a series of compounds with a constant metal. Such constancy is not expected because changing a unique ligand, for example, will change both the formal charge and the radial properties of the metal d orbitals, thus changing the σ and π interactions with a constant ligand. If the range over which a given ligand's σ and π parameters change is small compared to the difference between the values of the parameters of different ligands, then trends in the interactions of a series of ligands with a given metal can be interpreted.

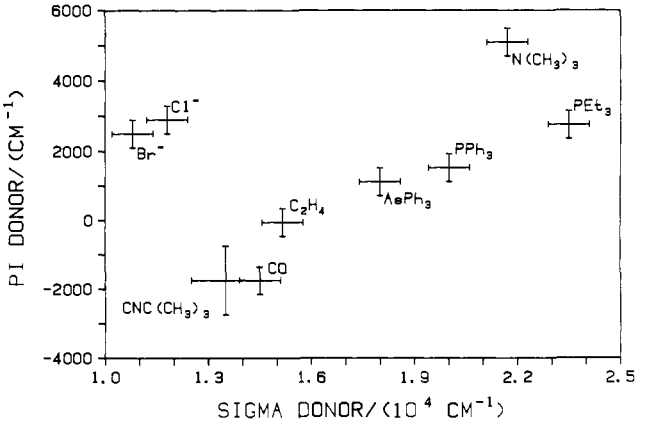

Figure 5. Two-dimensional spectrochemical series for the PtX_3L^{n-} complexes.

Experience with square-planar platinum(II) complexes has shown that the values of the parameters have an uncertainty which is estimated to be on the order of ±500 cm^{-1}. Several tests of this statement can now be made by using the chloro and bromo carbonyl compounds which are discussed here. The simplest test is to directly transfer the σ and π parameters for the carbonyl ligand which were determined from $PtCl_3CO^-$ and to transfer the σ and π parameters for Br^- which were determined from $PtBr_4^-$ in order to calculate the transition energies of $PtBr_3CO^-$. The results of this calculation are in very good agreement with the experimental transition energies reported in Table I. The average discrepancy was 380 cm^{-1} with the most poorly calculated transition energy, that of the $^1A_2$ state, being 640 cm^{-1} too large. When the values of the AOM parameters were varied in order to obtain the best fit (Table IV), the maximum change in any of the parameters which was needed was 100 cm^{-1}.

A similar test of the transferability of the parameters was made by using the ethylene parameters from $PtCl_3C_2H_4^-$ and the bromide parameters from $PtBr_4^{2-}$ to calculate the spectrum of $PtBr_3C_2H_4^-$. It was found that the σ parameters only needed to be changed by 40 cm^{-1} and the π parameters by 115 cm^{-1} in order to obtain the best fit.

The tests described above suggest that even in the case of covalent, back-bonding ligands, the angular overlap parameters can be transferred between compounds within limits of several hundred wavenumbers. Thus, based on the experiments performed to date, interpretation of trends in the σ and π interaction properties of ligands whose parameters differ by more than 1000 cm^{-1} is reliable.

Position of CO and $CNC(CH_3)_3$ in the Two-Dimensional Spectrochemical Series. The two-dimensional spectrochemical series for the ligands studied to date is shown in Figure 5. The series is shown as a plot of the π-donor vs. the σ-donor values which were determined by using the full energy matrix calculations. The uncertainties, indicated by the error bars, are small enough to allow the trends between most of the ligands to be clearly discerned. Of the ligands studied to date, carbon monoxide is the best π acceptor (poorest π donor) and triethylphosphine is the best σ donor. The σ donor parameters determined by the AOM calculation follow the order

$$PEt_3 > NMe_3 > PPh_3 > AsPh_3 > C_2H_4 \sim CNC(CH_3)_3 \geq CO > Cl > Br$$

The trends in the π-acceptor series are somewhat more difficult to interpret. Consider first only the ligands L in the $PtCl_3L^-$ series. For these ligands, the quantitative order of π-acceptor ability is $CO \sim CNC(CH_3)_3 > C_2H_4 > AsPh_3 > PPh_3 > PEt_3 > NMe_3$.

This order is generally that expected from the trends obtained from CO stretching frequencies in L-substituted carbonyl complexes. The position of the isonitrile is not accurately determined because of the overlapping of the absorption bands. It can only be concluded that the π-acceptor abilities are similar to those of the carbonyl ligand. It is a better π acceptor than any of the other ligands in Figure 5.

The position of the halides in the π series, taken at face value, is unexpected. They appear to be weaker π donors than expected. We and others have pointed out that the π parameter, which ultimately is traced back to the d_{xy}, d_{xz}, and d_{yz} orbital energies, is influenced by electrostatic interactions with ligand σ-donor orbital's lone pair of electrons.[18,26,27] Thus in the square-planar complexes, both the d_{xy} and the d_{xz} orbitals are raised in energy by the electrostatic interaction with a strong σ-donor ligand L, and vice versa. This type of interaction should be particularly evident when the e_σ values are very large as is the case for NMe_3 and PEt_3 and of correspondingly less importance when the e_σ values are relatively small as is the case for Cl^- and Br^-. A useful interpretation of the π-interaction properties can be obtained by considering the value of the AOM π parameter relative to that of the σ parameter, i.e., the value of e_π/e_σ.

When the ligands in Figure 5 are ordered in terms of this normalized π parameter, the order in terms of increasing π-acceptor (decreasing π donor) ability is $Cl = Br < NMe_3 < PEt_3 < PPh_3 < AsPh_3 < C_2H_4 < CNC(CH_3)_3 = CO$. This normalized series does not affect the relative positions of the strong π-acceptor ligands but does place the halides as poorer π acceptors than the ammine, the position it occupies in the high oxidation state "Werner" complexes.

Conclusions

The single-crystal polarized electronic absorption spectra of $(Pr_4N)[PtCl_3CO]$, $(Pr_4N)[PtBr_3CO]$, and $(Pr_4N)[PtCl_3CNC(CH_3)_3]$ have been obtained and assigned. The metal-carbonyl bond is strongly weakened in the excited state. A Franck-Condon analysis of the vibronic structure shows that the Pt-C bond is lengthened by 0.18 Å. The stretching frequency decreased by about 100 cm^{-1}. The σ and π interactions of carbon monoxide with a metal are determined for the first time from electronic spectroscopy and ligand-field theory. Carbon monoxide is a very strong π-acceptor ligand as expected. It is a surprisingly strong σ-donor ligand. It's σ interaction with the metal is larger than that of chloride and bromide and about equal to that of ethylene. It is a much weaker σ donor than phosphines or ammines. Its position in the two-dimensional spectrochemical series is shown in Figure 5.

Acknowledgment. The support of this research by the National Science Foundation is gratefully acknowledged.

(26) Byrn, M. P.; Katz, B. A.; Keder, N. L.; Levan, K. R.; Magurany, C. J.; Miller, K. M.; Pritt, J. W.; Strouse, C. E. *J. Am. Chem. Soc.* **1983**, *105*, 4916.
(27) Keeton, M.; Chou, B. F.; Lever, A. B. P. *Can. J. Chem.* **1971**, *49*, 192.

On the Mechanism of Stereoselective Epoxidation of Alkenes by Oxo-Iron Porphyrins

Karl Anker Jørgensen

Contribution from the Department of Organic Chemistry, Chemical Institute, Aarhus University, DK-8000 Aarhus C, Denmark. *Received March 12, 1986*

Abstract: The structure of oxo-iron porphyrins and their stereoselective epoxidation properties of alkenes are analyzed from a theoretical point of view. It is found that the most stable structure of oxo-iron porphyrin is one in which oxygen is inserted into the iron-nitrogen bond. This structure is equivalent to some of the carbene analogues, and the bond lengths for Fe-O (1.9 Å) and N-O (1.4 Å) are in good agreement with those found in the nickel analogue of **6**. The insertion of oxygen into the iron-nitrogen bond makes some of the d orbitals on iron available for interaction with the alkene; this type of complex is supported by recent experimental observations. The alkene can be coordinated in a perpendicular or parallel orientation at the iron atom (relative to the iron-oxygen bond), and the perpendicular orientation is found to be the most favorable. This binding of the alkene can then cause the stereoselective epoxidation properties, as the trans substituents will interact repulsively with the iron-porphyrin moiety. It is then suggested that the next step in the reaction mechanism is a slipping motion of the alkene toward the oxygen. This motion is controlled by a favorable interaction between the π^* orbital of the alkene and the lone pair on the oxygen which is antisymmetric with respect to the iron-oxygen-nitrogen plane. Aspects of this type of mechanism in relation to the experimental results as well as other transition metal catalyzed epoxidation reactions are discussed.

Iron functions as the principal electron carrier in biological oxidation-reduction reactions.[1] Iron also serves to transport and store molecular oxygen, a function that is essential to the life of all vertebrates.[1] As to the structure of the oxygen-iron bond in hemoglobin, Collman's group has found that oxygen binds in an end-on fashion (Pauling's model) to the iron of the protoheme, rather than in the sideways manner proposed by some theories.[2] Removal of an oxygen atom from hemoglobin leads to an oxo-iron(V) porphyrin, generally written as **1** (the hydrogen atoms are omitted for clarity), which is now generally accepted to be the active oxidant in P-450 monooxygenase, catalase, peroxidase,

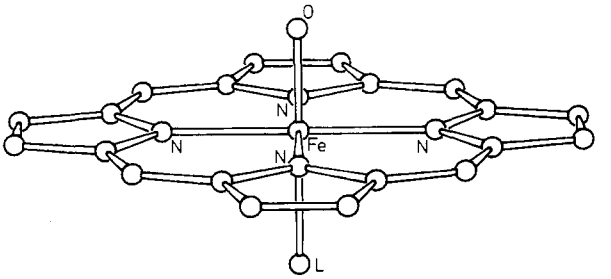

1

and chloroperoxidase.[3] **1** has also been shown to be a useful catalyst in oxidation reactions in organic synthesis.[4]

(1) See, e.g.: Dugas, H.; Penney, C. *Bioorganic Chemistry*; Springer-Verlag: New York, 1981; pp 346-362 and reference related to these pages.
(2) Collman, J. P. *Acc. Chem. Res.* **1977**, *10*, 265-272.

0002-7863/87/1509-0698$01.50/0